

Mechanisms for nonlinear refractive index in organic cavity polaritonsSamuel Schwab^{✉*} and William Christopherson*Physics Department, Case Western Reserve University, Cleveland, Ohio 44106, USA*

Robert Twieg

Department of Chemistry and Biochemistry, Kent State University, Kent, Ohio 44240, USA

Michael Crescimanno

*Department of Physics, Youngstown State University, Youngstown, Ohio 44555, USA*Kenneth Singer^{✉†}*Physics Department, Case Western Reserve University, Cleveland, Ohio 44106, USA*

(Received 8 April 2021; revised 23 July 2021; accepted 27 July 2021; published 18 August 2021)

The nonlinear optical response of organic polaritonic matter has received increasing attention due to their enhanced and controllable nonlinear response and their potential for novel optical devices such as compact photon sources and optical and quantum information devices. Using z scans at different wavelengths and incident powers we have studied the nonlinear optical dispersion of ultrastrongly coupled organic cavity polaritons near the lower polariton band. We show that the up to 150-fold enhancement of the nonlinear response compared to a cavityless organic film arises from an intensity-dependent polaritonic resonant frequency shift (“blueshift”). Consequently, we find that these z -scan data can only be described by several terms of a power series expansion in intensity whose respective contributions depend on power broadening and detuning from the lower polariton band. We further show that the nonlinear response can be quantitatively described by a semiclassical three-level molecular model coupled to the cavity in which saturation reduces the Rabi splitting, thus accounting for the lower polariton band’s observed blueshift.

DOI: [10.1103/PhysRevB.104.085307](https://doi.org/10.1103/PhysRevB.104.085307)**I. INTRODUCTION**

Cavity polaritons are light-matter mixed states arising from coupling between excitonic matter and confined light fields [1]. Being part exciton and part photon, polaritons are highly tunable and have thus inspired an emerging field for potential chemical and quantum engineering applications [2–4]. Already, a plethora of classical and quantum phenomena ranging from angle-dependent amplification [5], parametric oscillation [6], and enhanced emission [7,8] to single-quanta entanglement preservation [9], room-temperature out-of-equilibrium Bose-Einstein condensation [10], and superfluidity [11] have been found in polaritonic systems. Moreover, the ultrastrong coupling regime (where coupling energy compares to the band gap of material) opens up new avenues in tunability suitable for quantum and classical applications beyond the rotating-wave approximation [12,13].

Cavity polaritons made from Wannier-Mott excitons found in semiconductor structures have been studied extensively and typically fall within the strong coupling regime for light-matter interactions [14]. In organic materials, the large

oscillator strengths and binding energies of Frenkel excitons make ultrastrongly coupled polaritons easily attainable at room temperature even with low- Q mirrors. Further, the ease of adjusting the exciton-photon coupling through mixing of organic dyes with polymers adds an additional and useful tunability [12,15–17].

Exploration into the nonlinear optical properties of cavity polaritons has been fruitful. So far, enhanced and tunable third-harmonic generation [18–20], enhanced second-harmonic generation [21], and novel four-wave mixing processes [22] have been explored. These works suggest that the nonlinear response is dictated by the polariton states, instead of the intuitive material resonant states. In this work, we further elaborate on this picture for the sum-over-states model by investigating the complex intensity-dependent refractive index in ultrastrongly coupled organic polariton states using the z -scan technique [23,24] over ranges of pump wavelengths and powers. We measure a nearly 150-fold enhancement of the Kerr effect around the lower polariton (LP) resonance when compared to the bare excitonic film. We quantitatively show that optical saturation of the “bright” exciton reservoir leading to a blueshift of the LP band explains much of the experimentally observed behavior. A toy model using an intensity-induced shift of a single Lorentzian resonance indicates expected contributions of higher order nonlinear response to the intensity-dependent refractive index. A

*sxs1789@case.edu

†kds4@case.edu

semiclassical three-level optics model of the organic molecule coupled to a cavity mode quantitatively reproduces our z -scan observations. Notably, doing so with a three-level model only meaningfully introduces a single free parameter, an excited state mixing rate.

Background

Recently, polaritonic systems containing Frenkel excitons have been shown to exhibit strong blueshift in the LP when pumped around the threshold for creating a polariton condensate [25]. This shift has been primarily attributed to saturation and intermolecular energy migration. Although our experiments are at excitations below the condensate regime, we explore the effects of saturation on the detectable output of our samples in a z -scan configuration, displaying the pivotal role it plays in the nonlinear optical response.

As a toy model of how a resonance energy shift results in an intensity-dependent refractive index, consider a single-resonance Lorentzian dispersion with an intensity-dependence shift of the resonance frequency, descriptive of our experiments near the lower polariton resonance. Denote the associated population loss and dephasing rates as γ and γ_2 , and the product of the dipole matrix element connecting these two states and the exciting electric field by $E(t) = Ee^{-i\omega t} + \text{c.c.}$, with ω representing the input frequency. Solving the optical Bloch equations in the rotating-wave approximation for the steady state we arrive at the usual solution for the density matrix element associated with a transition between ground and excited state, ρ_{eg} . In the low intensity, low density limit, the real part of this solution gives the index of refraction as ($I = E^2$)

$$\begin{aligned} \text{Re}(\rho_{eg}) - 1 &= n - 1 = \frac{\omega N d^2 \delta}{2\epsilon_0 c k_0 (\delta^2 + \gamma_2^2 + 4\frac{\gamma_2^2}{\gamma} E^2)} \\ &\Rightarrow U(\omega) \frac{\delta + \tau I}{(\delta + \tau I)^2 + \Gamma^2 + P I}, \end{aligned} \quad (1)$$

where N represents the number density of the molecules, d their dipole matrix element, c the speed of light, k_0 is the vacuum wave vector, and $\delta = \omega - \omega_0$ is the detuning from resonance. We simplify the expression using $U(\omega)$, a prefactor depending on the oscillator strength, and anticipating its significance for this study, we introduce an intensity-dependent blueshift parameter, τ , into the detuning, $\delta \rightarrow \delta + \tau I$. We also introduce Γ as a decay rate and P as a power broadening parameter. Subsequently expanding Eq. (1) in powers of I reveals various orders of nonlinear optical response. Defining $\Delta n = n(I) - n(0)$,

$$\frac{\Delta n}{I} = n_2 + n_4 I + n_6 I^2, \quad (2)$$

where, for example,

$$n_2 = U(\omega) \frac{(\Gamma^2 - \delta^2)\tau - \delta P}{(\delta^2 + \Gamma^2)^2}. \quad (3)$$

Expressions for n_4 and n_6 are given in the Supplemental Material [26]. These expressions indicate that, due to the intensity dependence resonant shift (AC Stark effect), we expect our z -scan measurements to reflect not only optical Kerr re-

sponses, but also contributions from high order nonlinearities, and, moreover, to indicate how the various nonlinear orders depend on the excitation wavelength. Note in the limit of small blueshift ($\tau \approx 0$) the expansion of the nonlinear index leads to sign alternation between nonlinear indices $n_2 < 0$, $n_4 > 0$, $n_6 < 0$. In this limit, this two-level model also indicates a general qualitative trend; that with blueshift parameter (τ) each nonlinear term is not necessarily an odd function of the detuning from the resonance. This qualitative difference is salient below, as we use the three-level semiclassical model and compare with the experimental results. Lastly, to convert both experimental measurements and numerical evaluations of the theory model into this form we followed the prescription in Bindra *et al.* [27] and Said *et al.* [28], inferring n_2 , n_4 , and n_6 from that of the associated terms in the expansion of the intensity-dependent refractive index.

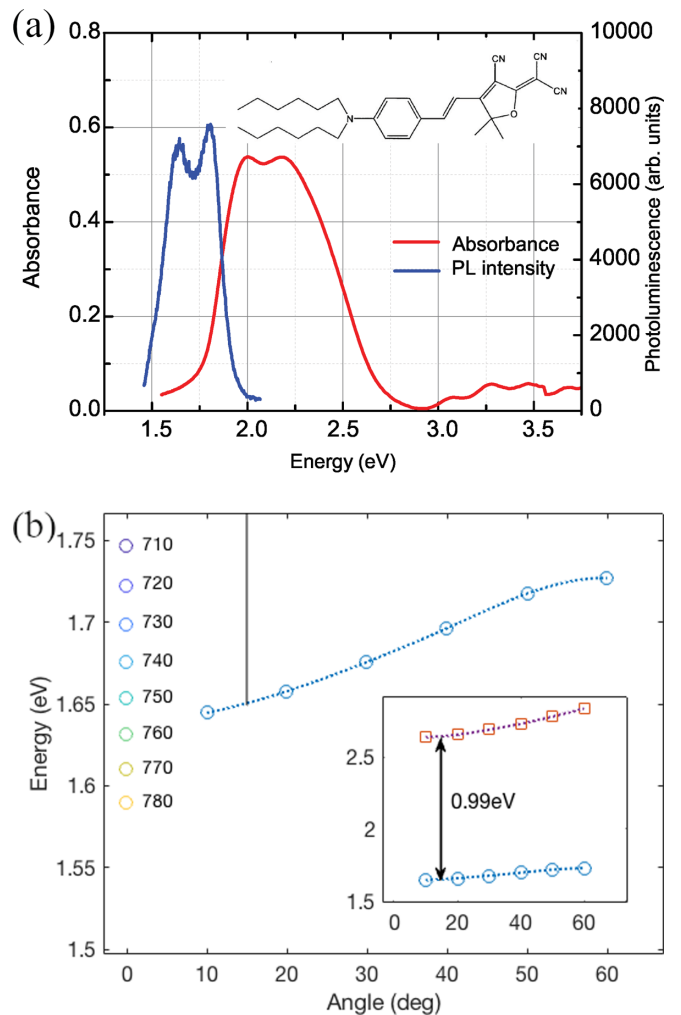


FIG. 1. (a) Absorption (red) and photoluminescence (blue) of DCDHF-6V. Chemical structure shown in the inset. (b) The main figure shows the LP dispersion (blue circles). For comparison, the experimental z -scan pump wavelengths from 710 to 780 nm are plotted on the same axis with dark to light circles at normal incidence. The inset displays both upper (red squares) and lower (blue circles) polariton bands, with Rabi splitting energy of about 1 eV located at 15° (vertical lines in both panels showing angle of degeneracy). Inset axes labels are the same as the main axes.

II. RESULTS AND DISCUSSION

The polariton low- Q samples were fabricated on glass substrates with thermally deposited Ag for reflectors. The active subwavelength medium is comprised of a 2:1 mass ratio of the organic dye molecule derivative of 2-dicyanomethylen-3-cyano-2,5-dihydrofuran (DCDHF)-6V [absorption and photoluminescence shown in Fig. 1(a)] and polymethyl methacrylate (PMMA). The organic film thickness was approximately 150 nm, and the silver film thickness approximately 20 nm corresponding to a cavity Q around 5. The linear optical dispersion derived from reflectivity spectra (Supplemental Material Fig. S1 [26]) of the entire structure is shown in Fig. 1(b) along with the pump wavelengths associated with the z -scan experiment. Our samples exhibit a Rabi splitting energy of 0.99 eV, placing them into the ultrastrong coupling regime.

A. Experimental results

The z -scan technique [23,24] consists of focusing a Gaussian laser field into a waist and translating the sample (the

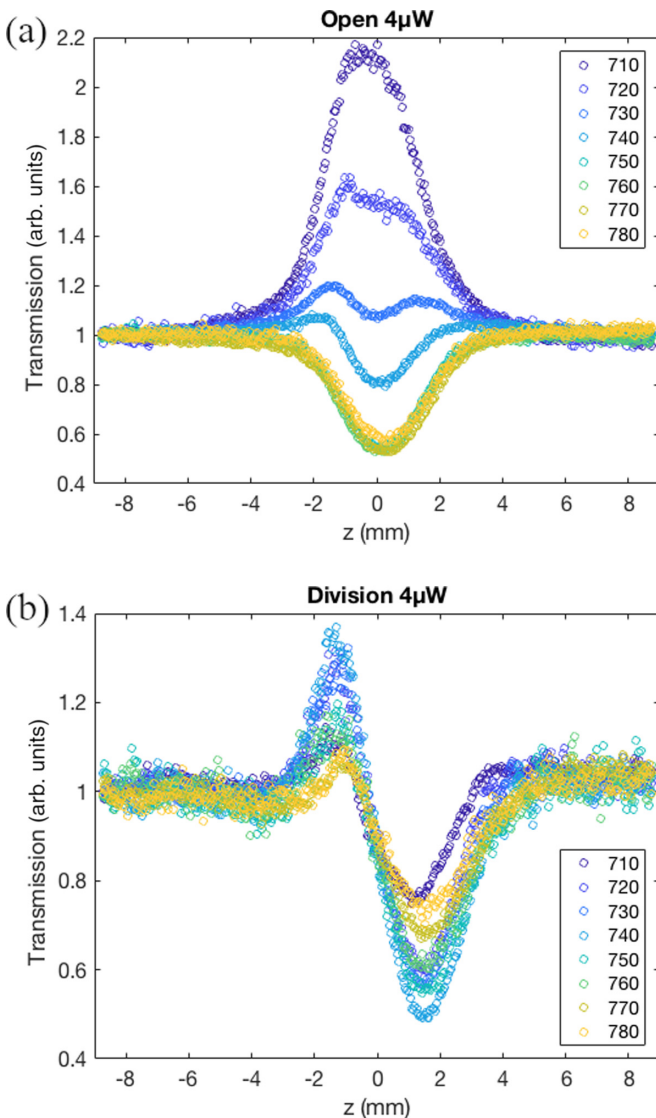


FIG. 2. (a) Normal incidence open aperture and (b) closed/open aperture z -scan data scanned at $4 \mu\text{W}$ average power at each respective wavelength.

cavity polariton slide) through that waist (see Fig. S2, Supplemental Material [26]). Downstream from the waist both the total light transmitted through the sample (the “open” z -scan signal) and light that arrives behind the collection lens strictly on axis (the “closed” z -scan signal) is recorded. The open signal indicates nonlinear absorption, whereas the ‘closed signal, since it is the light that has passed through a nearly closed iris, indicates a combination of nonlinear refraction and nonlinear absorption.

Z -scan measurements were taken at wavelengths on both sides of the nominal LP resonance and at various powers. The dominant feature of the open aperture was found to transition from enhanced to diminished transmission from the far-blue to the far-red side of the resonance, but in the intermediate region close to the polariton resonance we consistently measure a reentrant resonant feature indicating a mixture of the two as shown in Fig. 2(a). This reentrant resonant feature was present at all power levels, but its visibility for a specific pump wavelength increases with incident power. This reentrant feature arises as the incident intensity changes along the axial scan accentuating the competing processes. We measured a large response in the closed aperture detection arm indicating throughout a negative nonlinear refractive index for our system. To remove the effects of overall intensity change, we divide the closed aperture data and the open aperture data, also shown in Fig. 2(b), to obtain the real part of the intensity-dependent refractive index. For a baseline we measured the nonlinear response of a thick film of DCDHF-6V (~ 370 nm) (no mirrors and so no cavity polaritons) using the same preparation as the cavity polariton sample. We found the effective nonlinear index, n_2 , at 680 nm of this cavityless thick film to be $-1.58 \times 10^{-16} \text{ m}^2/\text{W}$. Experimental open and closed/open aperture data for this thick film are included in the Supplemental Material [26].

We also investigated the power-dependent nature of our responses to determine which high-order processes contribute to our data. Five average power levels were taken for all wavelengths from 710 to 780 nm. The overall transmission difference, from peak to valley, of the z -scan division are shown in the Supplemental Material [26], and the extracted $\Delta n/I$ are shown in Fig. 3(a). We see a general enhancement of the relative index change around the polariton resonance, but slightly blueshifted by about 10 nm. At higher powers this blueshift becomes larger. The nonlinear enhancement and evidence of higher-order effects is made apparent in the main panel of Fig. 3(a). The associated total index change ($\Delta n/I$) becomes diminished at higher power and indicates a high-order effect of opposite sign. It is worth noting that the intensity dependence and curvature in this graphic necessitates the inclusion of both n_4 and n_6 terms [see Eq. (2)].

Figure 3(b) shows the extracted nonlinear indices which result from fitting the $\Delta n/I$ data to an order-two polynomial to match that of Eq. (2). It indicates an up to 150-fold enhancement of n_2 of over $-2.5 \times 10^{-14} \text{ m}^2/\text{W}$ relative to the nonpolaritonic result of $-1.58 \times 10^{-16} \text{ m}^2/\text{W}$ as noted above. In addition, there is an apparent alternation of overall sign in these extracted indices with a roughly symmetrical enhancement around the polariton resonance. This also cross-checks with the appearance of the reentrant feature in the open z -scan (Fig. 2) according to Ref. [29], where they assert that it directly implies different signs for the n_2 and n_4 .

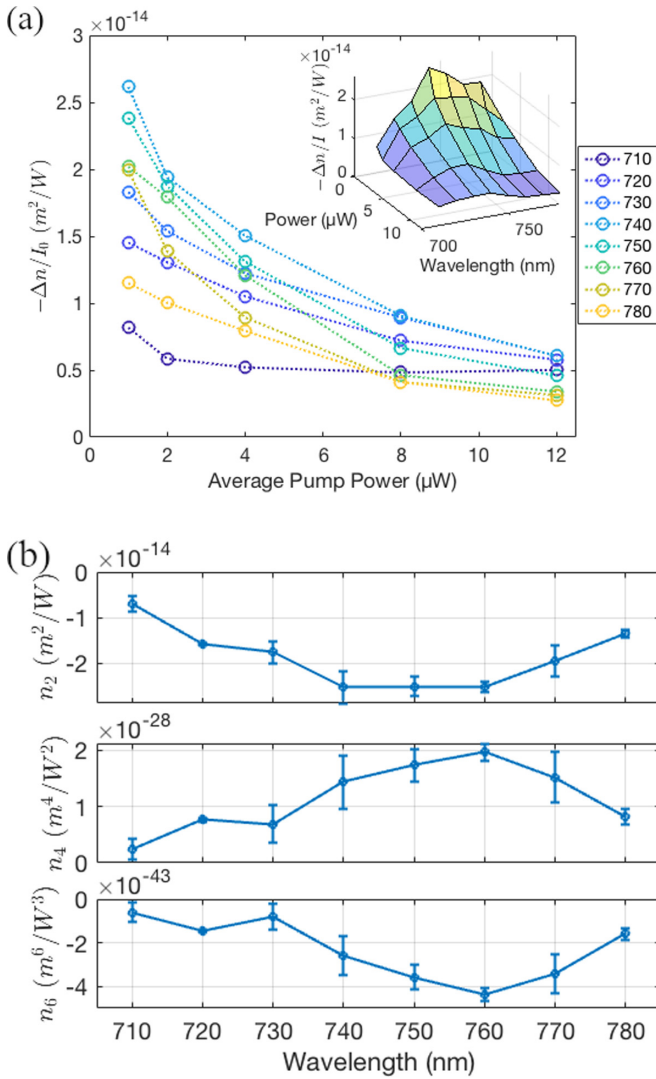


FIG. 3. (a) Trends with intensity for change in index/intensity, where each line corresponds to a pump wavelength in nanometers for various input intensities. Inset shows the surface plot of the same data, but highlights the enhancement around the polariton resonance. (b) Results from the fitting process of the data in panel (a) using an order-two polynomial fit. These parameters are effective n_2 , n_4 , and n_6 (top to bottom, respectively) of the system.

B. Discussion

1. Semiclassical model

Recently, it was shown in [19] that third-harmonic generation into the polariton branches has a dispersive character indicative of the polariton state rather than the exciton. In the sum-over-(intermediate) states picture of third-harmonic generation this fact indicates that the natural basis states for perturbation theory is not the exciton but the polaritons themselves. In a similar vein below, we explain the wavelength dependence of our more recent z -scan data also cannot be accommodated by a two-level model of the dye exciton. Further we show that, at minimum, a three-level model is necessary to connect with the experimental results.

In general, three-level models in a semiclassical perturbation expansion are the minimum for capturing the linear

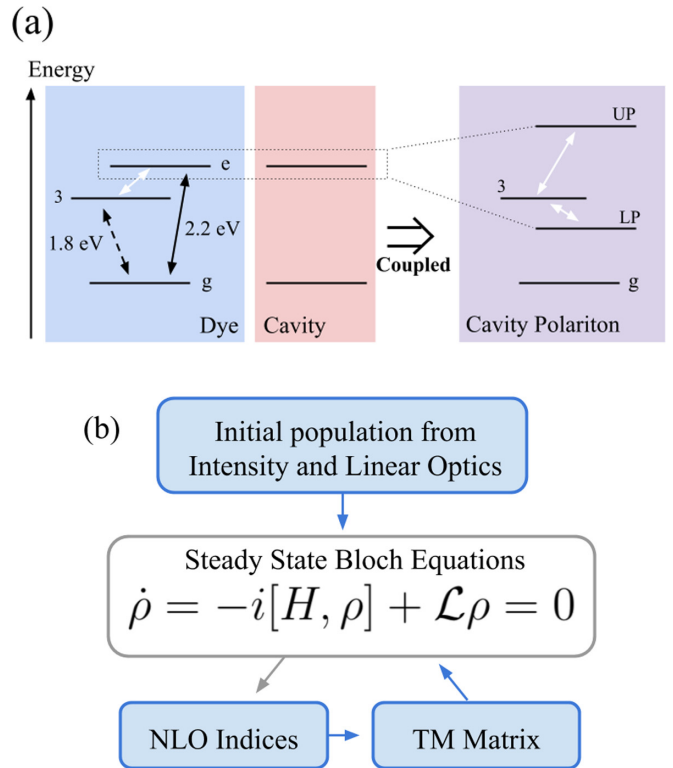


FIG. 4. (a) The individual excitons cooperatively couple to the cavity fields. The dispersion in their collective optical response splits the nearby cavity resonance into two states: The upper (“UP”) and lower (“LP”) polaritons. Black arrows are radiative transitions with the dotted arrow signifying the weak dipole matrix element; white are nonradiative mixing. (b) General flow diagram showing how the numerical evaluation of our polariton system embedded in a z -scan setup takes place. The self-consistent steady-state solution emerges from the final three blocks.

and leading nonlinear response such as nonlinear absorption [30–32]. Taking a cue from the absorption and photoluminescence curves of Fig. 1(a), our level scheme for the organic dye, displayed in Fig. 4(a), consists of a ground state connected by a large matrix element to an excited state centered at 600 nm (~ 2.1 eV, the exciton) and a third state at 660 nm (1.8 eV, we call the “third state” and labeled 3 in Fig. 4) above the ground state that itself only weakly radiatively decays to the ground state. As appropriate for a semiclassical optical model of the dye, the polariton states are not included in the model but emerge in the dye-loaded cavity system. Further, in addition to the radiative processes between each, the exciton or third state and the ground state, we include a fast nonradiative mixing between the third state and the exciton state. This describes significant rapid quenching of the exciton state into the third state. This establishes our reference three-level model. Note, however, that our study will conclude that the mixing parameter is most relevant for comparison with experiment and that we cannot actually determine the third state detuning from our data.

Since the absorption and relaxation processes are fast compared to the excitation pulsewidth (see Experimental section), it is sufficient to solve the associated three-level Bloch equations in steady state and use the coherences found in that

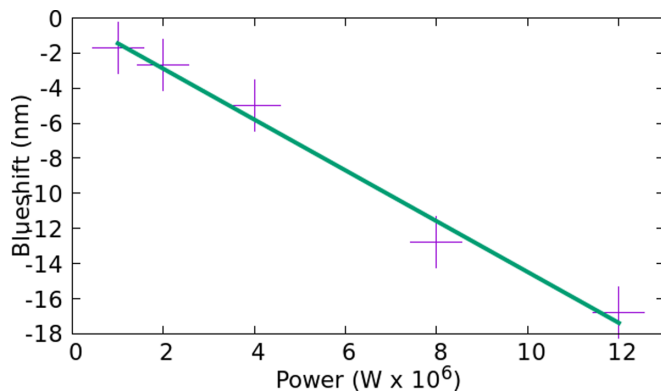


FIG. 5. The crossover wavelength as a function of incident power. The crossover wavelength is the pump at which the open z -scan at $z = 0$ has a transmission of 1 (matching large z), and we note it noticeably blueshifts with the power. Green curve is from evaluation of the theory and the points are experimental data. Note, this is not a fit.

limit to compute their contribution to the (complex, nonlinear) index of refraction for the dye layer. That index is then used in the transfer matrix modeling of the cavity polariton system. Note that to capture the nonlinear optical response of the system we must include intensity-dependent changes in the index which critically modify (spectral location and depth of) the polariton states “UP” and “LP.” We do so at each given wavelength and incident intensity by iteratively updating the cavity fields after recalculating the index and transfer matrices until a self-consistent (stationary) cavity intensity is achieved. The diagram in Fig. 4(b) is a schematic of this process, and more detail on the theory model and its evaluation is left for the Supplemental Material [26]. We numerically evaluate this model to emulate the z -scan experimental protocol.

2. Comparison to experiment

Much of the observed z -scan data delineating the nonlinear response in ultrastrongly coupled organic cavity polaritons results from a single physical effect: The optical saturation of the dye. The remaining observations beyond this simple description are experimental evidence for the necessity of including the effects of a third nonradiative level (third state) in the underlying model of the dye. In this section, we show how our model matches the experimentally measured blueshift, and then compare theoretical and experimental open and closed aperture signals. We then compare the effective nonlinear response as a function of wavelength and incident intensity through a comparison of extracted nonlinear indices as introduced in Eq. (2).

In Fig. 5 we show at various power levels what we will call the “crossover wavelength.” For a given power level, there exists one pump wavelength whose z -scan will give a normalized transmission of 1 at its center. At low power, there is a smooth transition between nonlinear absorption and saturable absorption (SA)-like behavior and so the crossover wavelength will have an overall flat z -scan shape. At higher powers, the trace will have more prominent “m-shaped” features and the crossover wavelength is the pump wavelength whose middle of the “m” touches the $T(z) = 1$ line. This

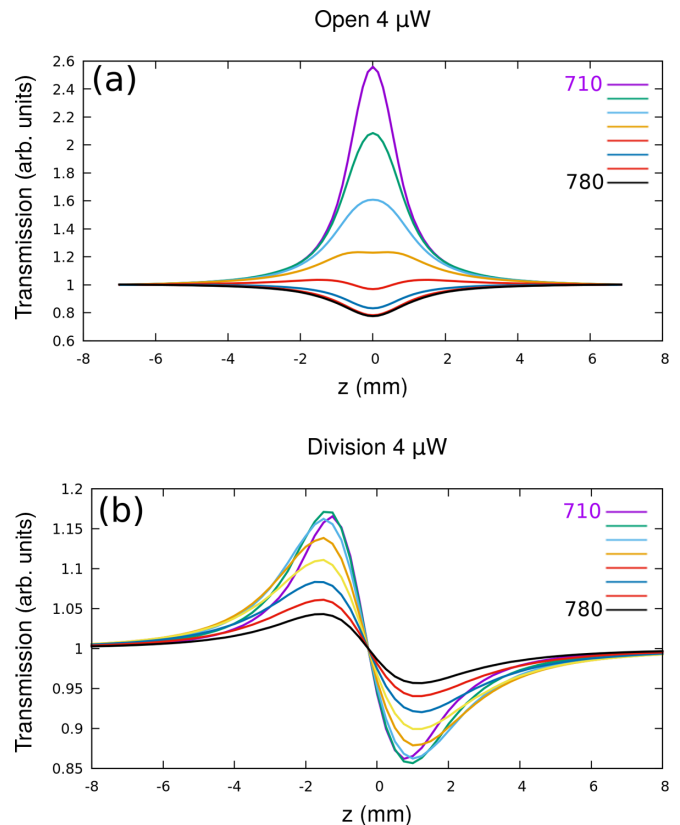


FIG. 6. (a) Open z -scan theory traces. (b) Closed/open z -scan theory curves. Legend indicates traces from 710–780 nm, each 10 nm apart as in Fig. 2. Mixing rate set to $4 \times 10^5 \text{ s}^{-1}$ between the exciton and the third state. Compare with experimental Fig. 2, though these theory simulations used $4 \mu\text{W}$ of optical power.

crossover point quantifies the blueshift of our system, and we find strong agreement between the trends in both experiment and theory. More information on this process is discussed in the Supplemental Material [26].

Our three-level semiclassical model for the dye has essentially a single free parameter; the mixing among the third state and the exciton state. This parameter changes the dispersive character of the optical saturation of the dye. For a particular mixing rate, we evaluate the full model and compare the open and closed/open channels in both theory and experiment. Shown in Fig. 6 is a result of our three-level model. We note here the qualitative comparison to the experiment in Fig. 2 in both the open and division data. There are three main qualitative features in the open aperture data and two main features in the division data we will compare. We will also discuss how they are the result of optical saturation for the open z -scan data for these ultrastrongly coupled organic cavity polaritons.

(1) SA to nonlinear absorption (NA) transition: As seen in Figs. 2 and 6, scanning in wavelength across the polariton resonance(s), the open z -scan data change by processes similar to SA-like (reduced nonlinear absorption) to nonlinear absorption. The wavelength at which this transition occurs shifts blue with increasing intensity, which follows the same trend as depicted in Fig. 5.

Saturation due to the brightening of the internal cavity optical fields reduces the cavity coupling. This reduces the vacuum Rabi frequency, reducing the gap between the polariton resonances [33]. This causes the UP to move to longer wavelengths and the LP to shorter (“blueshift”). Theory model evaluations of this are included in Supplemental Material Fig. S5. At low intensities (linear optical regime), the polariton resonances increase the intracavity intensity. Thus, if blue detuned from the LP, then during the intensity increase in a z -scan the LP moves towards the drive wavelength, resulting in SA-type behavior in the open z -scan channel. The same blueshift causes an intensity decrease when the LP is scanned at a red detuned wavelength, thus appearing as NA. If saturation dominates we would expect exactly the opposite behavior crossing the UP, which indeed is indicated by our experimental findings (see Fig. S6). Note these findings cannot be reproduced by a simple wavelength-independent nonlinear index for the dye, because in that case both UP’s and LP’s intensity-dependent frequency shift would have the same sign, as indicated in Eq. (3). Also, we ruled out the influence of the dye photobleaching over time by comparing multiple data sets of the power series and ensuring that there was no temporal response.

(2) The reentrant (“M”-shaped) feature in the middle of the SA-NA transition: Also apparent from Fig. 2 is that the open aperture signal has a reentrant behavior at wavelengths in the transitions from the SA to NA. With increasing optical power this reentrant transition feature for the LP blueshifts in wavelength, broadens about z , and increases in contrast.

As a result of the blueshift of the LP with intracavity intensity, the LP resonance center shifts so far that it passes to the blue of the excitation wavelength itself. In that case the absorption first decreases at $z \neq 0$ as the blueshift pulls the LP resonance towards it and then appears to increase as $z \rightarrow 0$ since there it continues to blueshift the LP so far that at that wavelength the scan goes off resonance again *on the long wavelength side*. We note that there is a rich literature of such transition features [34–40] in open z -scan data, and in all cases the feature is a consequence of intensity-dependent frequency pulling of an optical resonance of some sort. This picture also explains the increased broadening in z -scan coordinate, increased contrast with power, and implies that the same phenomenology of the reentrant transition feature should appear red of the UP, which we have also verified experimentally (Fig. S6).

(3) The nonlinear absorption behavior in the open aperture data of the LP persists far into red detuning, to nearly 100 nm beyond the LP. This appears to not be a simple consequence of saturation; instead, we understand this behavior as consequent to the active participation of a third level in the semiclassical model of the dye. The participation of this third level through its rapid mixing with the exciton furnishes a longer-lived set of metastable states that do not themselves directly lead to cavity pulling, but through excited state mixing, broaden the frequency response of the dye at high intensity.

As described in the Supplemental Material, the laser power, beam profile, z -scan optics chromatism, and detection chain were well characterized and those measured parameters were used in connecting theory outputs (self-consistent nonlinear optical transfer matrices) to the associated open- and closed-

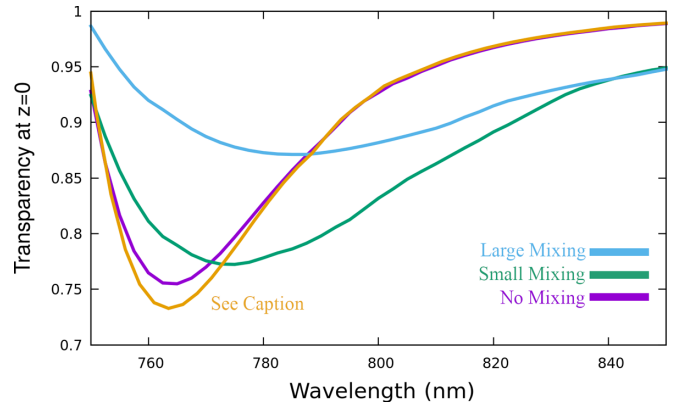


FIG. 7. Theory open z -scan minima as a function of wavelength; all parameters in the model are the same except the mixing rate between the exciton and the third state as described in the text. Power is $4 \mu\text{W}$ for blue, green, and purple curves. The purple curve is the two-state model (no mixing), the green is for a mixing rate of $4 \times 10^5 \text{ s}^{-1}$, and the light-blue curve is with a mixing rate of $8 \times 10^5 \text{ s}^{-1}$. The gold curve is the square of the two-state (no mixing) model at half the power, showing that changing the power cannot explain the observed persistence of the additional nonlinear absorption red of the LP.

signal channels. Also described there are how all but one of the relevant microphysical parameters of the semiclassical model of the dye are fixed by the linear optical behavior and dye density. Thus the non-Hermitian mixing rate between the third state and the exciton state is the only adjustable parameter in the model. Of course, two-photon absorption could also result in the pronounced nonlinear absorption, but the experimental lack of any clear dispersive character of the nonlinear absorption over this broad range of wavelengths appears to vitiate that explanation. The z -scan measurements we have compiled on these polaritonic media unfortunately do not unequivocally determine a particular dye energy level or coupling scheme; our so-called “reference model” [Fig. 4(a)] is simple and quantitatively useful but not the only possible explanation for our observations. A different set of experiments and more detailed quantum chemistry calculations are likely to be helpful in achieving a more complete picture here.

We directly, quantitatively compare a two-level (no mixing) and three-level model (with mixing) for the dye cavity polaritons in Fig. 7 by comparing open z -scan minima. Plotting these minima of the theory open z scan (i.e., at $z = 0$) as a function of detuning from the LP for different choices of that mixing rate allows a quantitative comparison with experiment. We therefore adopt a mixing rate of $4.0 \times 10^5 \text{ s}^{-1}$ in all the numerical evaluations of the theory model here except where noted otherwise. This provides evidence for the necessity of a three-level semiclassical model as minimal for understanding the relevant contributions from the dye nonlinear optical properties, seen here in its nonlinear optical effect of the associated ultrastrongly coupled cavity polaritons.

Having related each observed open z -scan feature qualitatively to the dye semiclassical model, we now use it in the qualitative explanation of the closed z -scan signal, by focusing on two defining features.

(1) The sign of Δn , the overall intensity-dependent refractive index: The observed closed z -scan signal from the cavity LP correspond to $\Delta n < 0$ for all wavelengths and powers. The magnitude of the effect increases as one approaches the blueshifted LP center wavelength, and broadens (in z -scan coordinate z) with power.

This is a consequence of the fact that the LP is below the exciton. Even in a two-level system, again as a consequence of power broadening/saturation, the first contribution to Δn is expected to follow that of normal dispersion, being negative at detunings below the exciton and positive above, as indicated by our experimental findings at the UP (not included here). The broadening seen is consistent with the expected power dependence of the nonlinear response, and we have already shown that its observed blueshift with power is quantitatively consistent with that due to the saturation depolarization of the dye in the cavity optical field.

(2) The z -scan shape changes and dynamic range of the closed/open z -scan with power: As noted, Δn from the closed z scan stays negative across the LP, but its magnitude changes with power differently at various detunings.

The sign of Δn does not tell the whole story. The magnitude of the Δn depends on detuning and fluence in such a way as to indicate the vital contribution of higher-order nonlinear susceptibilities. As described in the Experimental section [Fig. 3(b)] and as rendered from theory evaluation in Fig. 8 below, these changes can be recorded as nonlinear contributions to the index, n_i , $i = 2, 4, 6$. Qualitatively all three of these show dependence on the detuning (from the polariton) that is a consequence of a blueshift, as indicated qualitatively by expanding out the expression for n_i from Eq. (1). When we evaluate our model using the same methods as described in the Experimental section for extracting $\Delta n/I$, we find significant similarity. Namely, an enhanced response around the polariton resonance, and a change of sign for each higher-order effective nonlinear index, as seen in Fig. 8 and in the data of Fig. 3(b). The general broadening of the response movement to the blue at higher intensities is consistent with what was observed in the experiment, as is the significant agreement in the overall magnitude of the nonlinear response.

III. CONCLUSION

We have carried out experimental and theoretical studies of the nonlinear optical response spectrum of ultrastrongly coupled organic cavity polaritons. We find up to 150-fold enhancement of the response compared to cavityless films. Our experimental findings and their accompanied theoretical elucidation using a straightforward semiclassical three-level optics model, with essentially only a single adjustable parameter, indicates that for ultrastrongly coupled organic polaritons, the nonlinear refractive index is dominated by one main effect: The reduction of the vacuum Rabi frequency due to the saturation depolarization of the medium in the cavity's intense optical field. This reduction of Rabi frequency produces a blueshift of the LP yielding a complex nonlinear refractive index exhibiting contributions from higher-order contributions to Δn dependent on the detuning and power broadening as we show with a simple two-level model. Although the reduction of the Rabi frequency due to saturation

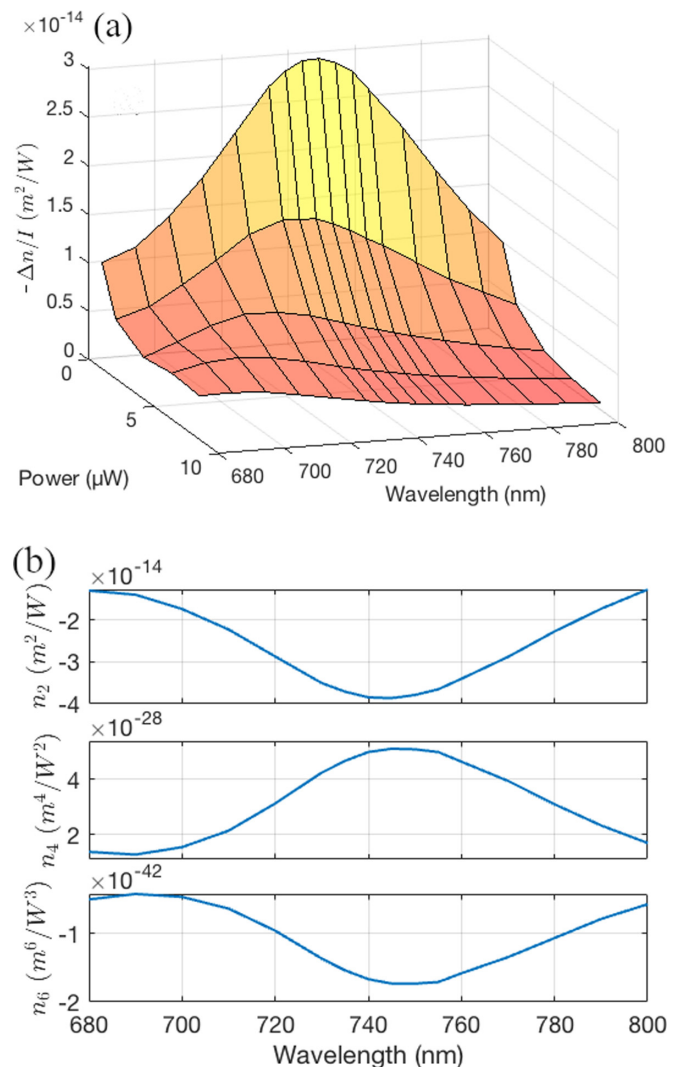


FIG. 8. (a) The theory-derived $\Delta n/I$ traces from theory closed/open theory. Parameters same as in Fig. 6. For (b) we converted the data in (a) into the intensity-dependent contributions to the overall index of refraction of the sample. Compare with experimental Fig. 3.

with intensity would also readily occur were there only two contributing levels, we find that the experimentally measured behavior of the open aperture behavior at long wavelengths further from resonance (longer than the LP) indicates mixing with a third level in our quantum description of the dye.

Although that latter point is not necessarily surprising, here we have done more by actually qualitatively and quantitatively connecting the underlying microphysical sources of the nonlinearities to those of the more complicated optical geometry. Further work is underway to delineate how dye-intrinsic higher-order nonlinear optical processes contribute to the observed z -scan signals.

Beyond being simply explanatory, we can use this model and understanding as a tool to predict and manipulate the nonlinear properties of multipolariton systems, which may be of practical utility for optical switching and quantum information processing using polaritonic matter.

ACKNOWLEDGMENTS

The authors acknowledge the use of the Materials for Opto/Electronics Research and Education Center (MORE) for sample preparation and characterization at Case Western Reserve University. The authors acknowledge the funding of this work from the National Science Foundation (Grant No. 1609077).

APPENDIX: EXPERIMENTAL SECTION

1. Sample fabrication

Samples were constructed on optically cleaned glass slides by first thermally depositing ~ 20 nm of Ag directly onto the glass. Following this, samples were spun coat with a 2:1 mass ratio of DCDHF-6V:PMMA mixture with a solvent of toluene (15 mg/ml concentration of dye molecule). This gave a sub-wavelength thickness to the dye layer of ~ 150 nm. Finally, the optical cavity is completed by thermally depositing the last 20-nm Ag layer atop the dye. The thickness of each layer is individually cross referenced with a control by removing a small patch of deposited material from the substrate and using a Tencor P6 stylus profilometer. In addition, an identical optical cavity filled with PMMA was constructed to observe the quality factor of the structure, which was found to be around 5.

2. Sample characterization

After fabrication, the linear optics of the samples were gathered using an angle-resolved spectrophotometer (Cary 6000i) at 10° increments from 10° to 60° . This characterizes the dispersion of the sample, and with fitting the curves we find the degeneracy point at about 15° from normal incidence. This Rabi splitting energy is found to be $\Omega_R = 0.99$ eV. This puts our cavity polariton samples well into the ultrastrong coupling regime.

3. Nonlinear index studies

Nonlinear index experiments were conducted using a parametric amplifier (TOPAS) pumped by a 200-fs laser system (Clark MXR) with a repetition rate of 1 kHz. The closed and open aperture z scans were recorded simultaneously and the experimental design is depicted in the Supplemental Material [26]. The samples were illuminated with average powers of 1, 2, 4, 8, and 12 μ W (peak intensity of 0.6, 1.2, 2.4, 4.8, and 7.2 GW/cm^2) and their associated open and closed aperture transmissions were recorded using Si large area biased photodetectors (Thorlabs Det100A2). The data were recorded every 50 μ m over 20 mm centered around the focus of the Gaussian beam (confirmed with Thorlabs BP-109 profiler) using a translation stage, then the data were centered through calibration with the translation stage in post. For each trace, the data were averaged over 30 pulses at each spatial point in addition to averaging over four total z scans conducted back and forth through the focus.

-
- [1] D. Sanvitto and S. Kéna-Cohen, The road towards polaritonic devices, *Nat. Mater.* **15**, 1061 (2016).
- [2] C. Schneider, K. Winkler, M. D. Fraser, M. Kamp, Y. Yamamoto, E. A. Ostrovskaya, and S. Höfling, Exciton-polariton trapping and potential landscape engineering, *Rep. Prog. Phys.* **80**, 016503 (2017).
- [3] I. Carusotto and C. Ciuti, Quantum fluids of light, *Rev. Mod. Phys.* **85**, 299 (2013).
- [4] D. S. Dovzhenko, S. V. Ryabchuk, Y. P. Rakovich, and I. R. Nabiev, Light-matter interaction in the strong coupling regime: Configurations, conditions, and applications, *Nanoscale* **10**, 3589 (2018).
- [5] P. G. Savvidis, J. J. Baumberg, R. M. Stevenson, M. S. Skolnick, D. M. Whittaker, and J. S. Roberts, Angle-Resonant Stimulated Polariton Amplifier, *Phys. Rev. Lett.* **84**, 1547 (2000).
- [6] L. Ferrier, S. Pigeon, E. Wertz, M. Bamba, P. Senellart, I. Sagnes, A. Lemàtre, C. Ciuti, and J. Bloch, Polariton parametric oscillation in a single micropillar cavity, *Appl. Phys. Lett.* **97**, 031105 (2010).
- [7] D. Ballarini, M. De Giorgi, S. Gambino, G. Lerario, M. Mazzeo, A. Genco, G. Accorsi, C. Giansante, S. Colella, S. D'Agostino, P. Cazzato, D. Sanvitto, and G. Gigli, Polariton-induced enhanced emission from an organic dye under the strong coupling regime, *Adv. Opt. Mater.* **2**, 1076 (2014).
- [8] A. M. Berghuis, A. Halpin, Q. Le-Van, M. Ramezani, S. Wang, S. Murai, and J. Gómez Rivas, Enhanced delayed fluorescence in tetracene crystals by strong light-matter coupling, *Adv. Funct. Mater.* **29**, 1901317 (2019).
- [9] Á. Cuevas, J. C. L. Carreño, B. Silva, M. De Giorgi, D. G. Suárez-Forero, C. S. Muñoz, A. Fieramosca, F. Cardano, L. Marrucci, V. Tasco, G. Biasiol, E. Del Valle, L. Dominici, D. Ballarini, G. Gigli, P. Mataloni, F. P. Laussy, F. Sciarrino, and D. Sanvitto, First observation of the quantized exciton-polariton field and effect of interactions on a single polariton, *Sci. Adv.* **4**, eaao6814 (2018).
- [10] K. S. Daskalakis, S. A. Maier, R. Murray, and S. Kéna-Cohen, Nonlinear interactions in an organic polariton condensate, *Nat. Mater.* **13**, 271 (2014).
- [11] G. Lerario, A. Fieramosca, F. Barachati, D. Ballarini, K. S. Daskalakis, L. Dominici, M. De Giorgi, S. A. Maier, G. Gigli, S. Kéna-Cohen, and D. Sanvitto, Room-temperature superfluidity in a polariton condensate, *Nat. Phys.* **13**, 837 (2017).
- [12] A. Frisk Kockum, A. Miranowicz, S. De Liberato, S. Savasta, and F. Nori, Ultrastrong coupling between light and matter, *Nat. Rev. Phys.* **1**, 19 (2019).
- [13] P. Forn-Díaz, L. Lamata, E. Rico, J. Kono, and E. Solano, Ultrastrong coupling regimes of light-matter interaction, *Rev. Mod. Phys.* **91**, 025005 (2019).
- [14] S. M. H. Luk, J. Keeling, F. M. Marchetti, M. H. Szymaska, and P. B. Littlewood, Collective coherence in planar semiconductor microcavities, *Semicond. Sci. Technol.* **22**, R1 (2007).
- [15] B. Liu, P. Rai, J. Grezmał, R. J. Twieg, and K. D. Singer, Coupling of exciton-polaritons in low- Q coupled microcavities

- beyond the rotating wave approximation, *Phys. Rev. B* **92**, 155301 (2015).
- [16] A. A. Anappara, S. De Liberato, A. Tredicucci, C. Ciuti, G. Biasiol, L. Sorba, and F. Beltram, Signatures of the ultrastrong light-matter coupling regime, *Phys. Rev. B* **79**, 201303(R) (2009).
- [17] S. Gambino, M. Mazzeo, A. Genco, O. Di Stefano, S. Savasta, S. Patanè, D. Ballarini, F. Mangione, G. Lerario, D. Sanvitto, and G. Gigli, Exploring light-matter interaction phenomena under ultrastrong coupling regime, *ACS Photonics* **1**, 1042 (2014).
- [18] F. Barachati, J. Simon, Y. A. Getmanenko, S. Barlow, S. R. Marder, and S. Kéna-Cohen, Tunable third-harmonic generation from polaritons in the ultrastrong coupling regime, *ACS Photonics* **5**, 119 (2018).
- [19] B. Liu, M. Crescimanno, R. J. Twieg, and K. D. Singer, Dispersion of third-harmonic generation in organic cavity polaritons, *Adv. Opt. Mater.* **7**, 1801682 (2019).
- [20] K. Wang, M. Seidel, K. Nagarajan, T. Chervy, C. Genet, and T. Ebbesen, Large optical nonlinearity enhancement under electronic strong coupling, *Nat. Commun.* **12**, 1486 (2021).
- [21] T. Chervy, J. Xu, Y. Duan, C. Wang, L. Mager, M. Frerejean, J. A. W. Mü, P. Tinnemans, J. A. Hutchison, C. Genet, A. E. Rowan, T. Rasing, and T. W. Ebbesen, High-efficiency second-harmonic generation from hybrid light-matter states, *Nano Lett.* **16**, 7352 (2016).
- [22] M. Romanelli, C. Leyder, J. P. Karr, E. Giacobino, and A. Bramati, Four Wave Mixing Oscillation in a Semiconductor Microcavity: Generation of Two Correlated Polariton Populations, *Phys. Rev. Lett.* **98**, 106401 (2007).
- [23] M. Sheik-bahae, A. A. Said, and E. W. Van Stryland, High-sensitivity, single-beam n_2 measurements, *Opt. Lett.* **14**, 955 (1989).
- [24] E. W. Van Stryland and M. Sheik-Bahae, Z-Scan Measurements of Optical Nonlinearities, *Characterization Techniques and Tabulations for Organic Nonlinear Materials*, edited by M. G. Kuzyk and C. W. Dirk (Marcel Dekker, New York, 1998), p. 655.
- [25] T. Yagafarov, D. Sannikov, A. Zasedatelev, K. Georgiou, A. Baranikov, O. Kyriienko, I. Shelykh, L. Gai, Z. Shen, D. Lidzey, and P. Lagoudakis, Mechanisms of blueshifts in organic polariton condensates, *Commun. Phys.* **3**, 18 (2020).
- [26] See Supplemental Material at <http://link.aps.org/supplemental/10.1103/PhysRevB.104.085307> for details of the linear optics of the system, modeling specifics, and comparison to pure film, which includes Ref. [41].
- [27] K. S. Bindra, S. M. Oak, and K. C. Rustagi, Intensity dependence of Z-scan in semiconductor-doped glasses for separation of third and fifth order contributions in the below band gap region, *Opt. Commun.* **168**, 219 (1999).
- [28] A. A. Said, M. Sheik-Bahae, D. J. Hagan, T. H. Wei, J. Wang, J. Young, and E. W. Van Stryland, Determination of bound-electronic and free-carrier nonlinearities in ZnSe, GaAs, CdTe, and ZnTe, *J. Opt. Soc. Am. B* **9**, 405 (1992).
- [29] B. Gu, J. Chen, Y. Fan, J. Ding, and H. Wang, Theory of Gaussian beam z scan with simultaneous third- and fifth-order nonlinear refraction based on a Gaussian decomposition method, *J. Opt. Soc. Am. B* **22**, 2651 (2005).
- [30] C. W. Dirk, I. T. Cheng, and M. Kuzyk, A simplified three-level model describing the molecular third-order nonlinear optical susceptibility, *Int. J. Quantum Chem.* **43**, 27 (1992).
- [31] E. Zojer, W. Wenseleers, P. Pacher, S. Barlow, M. Halik, C. Grasso, J. W. Perry, S. R. Marder, and J.-L. Brédas, Limitations of essential-state models for the description of two-photon absorption processes: The example of bis(dioxaborine)-substituted chromophores, *J. Phys. Chem. B* **108**, 8641 (2004).
- [32] J.-L. Bredas, C. Adant, P. Tackx, and A. Persoons, Third-order nonlinear optical response in organic materials: Theoretical and experimental aspects, *Chem. Rev.* **94**, 243 (1994).
- [33] T. B. Norris, J.-K. Rhee, D. S. Citrin, M. Nishioka, and Y. Arakawa, Coherent and incoherent dynamics of excitons in semiconductor microcavities, *Nuovo Cimento D* **17**, 1295 (1995).
- [34] Y. Gao, W. Wu, D. Kong, L. Ran, Q. Chang, and H. Ye, Femtosecond nonlinear absorption of Ag nanoparticles at surface plasmon resonance, *Physica E* **45**, 162 (2012).
- [35] X.-L. Zhang, Z.-B. Liu, X.-C. Li, Q. Ma, X.-D. Chen, J.-G. Tian, Y.-F. Xu, and Y.-S. Chen, Transient thermal effect, nonlinear refraction and nonlinear absorption properties of graphene oxide sheets in dispersion, *Opt. Express* **21**, 7511 (2013).
- [36] N. Dong, Y. Li, Y. Feng, S. Zhang, X. Zhang, C. Chang, J. Fan, L. Zhang, and J. Wang, Optical limiting and theoretical modelling of layered transition metal dichalcogenide nanosheets, *Nat. Sci. Rep.*, **5** 14646 (2015).
- [37] J. M. P. Almeida, G. F. B. Almeida, L. Boni, and C. R. Mendonça, Nonlinear optical properties and femtosecond laser micromachining of special glasses, *J. Braz. Chem. Soc.* **26**, 2418 (2015).
- [38] J. Olesiak-Banska, M. Waszkielewicz, K. Matczyszyn, and M. Samoc, A closer look at two-photon absorption, absorption saturation and nonlinear refraction in gold nanoclusters, *RSC Adv.* **6**, 98748 (2016).
- [39] Y.-X. Zhang and Y.-H. Wang, Nonlinear optical properties of metal nanoparticles: A review, *RSC Adv.* **7**, 45129 (2017).
- [40] C. Torres-Torres, J. Bornacelli, B. Can-Uc, H. G. Silva-Pereyra, L. Rodriguez-Fernández, M. Avalos-Borja, G. J. Labrada-Delgado, J. C. Cheang-Wong, R. Rangel-Rojo, and A. Oliver, Coexistence of two-photon absorption and saturable absorption in ion-implanted platinum nanoparticles in silica plates, *J. Opt. Soc. Am. B* **35**, 1295 (2018).
- [41] K. M. McPeak, S. V. Jayanti, S. J. P. Kress, S. Meyer, S. Iotti, A. Rossinelli, and D. J. Norris, Plasmonic films can easily be better: Rules and recipes, *ACS Photonics* **2**, 326 (2015).